



The impact of spatiotemporal patterns of land use land cover and land surface temperature on an urban cool island: a case study of Bengaluru

Nithya R. Govind · H. Ramesh

Received: 16 October 2018 / Accepted: 1 April 2019 / Published online: 16 April 2019
© Springer Nature Switzerland AG 2019

Abstract In most of the developing countries, man-made developments in the environment have led to the growing demand to contextualize the land use land cover (LULC) changes and land surface temperature (LST) variations. Due to the modification in the surface properties of the cities, a difference in energy balance between the cities and its nonurban surroundings is observed. The aim of this study is to analyze the spatial and temporal patterns of LULC and LST and its inter-relationship in Bengaluru urban district, India, during the period from 1989 to 2017 using remote sensing data. Intensity analysis was performed for the interval to analyze the LULC change and identify the driving forces. The impact of LULC change on LST was assessed using hot spot analysis (Getis–Ord G_i^* statistics). The results of this study show that (a) dominant LULC change experienced is the increase in urban area (approximately 40%) and the rate of land use change was faster in the time period 1989–2001 than 2001–2017; (b) the major transition witnessed is from barren and agricultural land to urban; (c) over the period of 28 years, LST patterns for different land use classes exhibit an increasing trend with an overall increase of approximately 6 °C and the mean LST of urban area increased by about 8 °C; (d) LST pattern change can be effectively analyzed using hot spot analysis; and (e) as

the urban expansion occurs, the cold spots have increased, and it is mainly clustered in the urban area. It confirms the presence of an urban cool island effect in Bengaluru urban district. The findings of this work can be used as a scientific basis for the sustainable development and land use planning of the region in the future.

Keywords Land use land cover · Land surface temperature · Intensity analysis · Urban cool island · Bengaluru

Introduction

Land use land cover (LULC) is identified as one of the key aspects of environmental change in both global and regional levels. The multifaceted interactions between human and physical environments lead to the process of LULC change (Manandhar et al. 2010; Huang et al. 2012). Quantification of the causes and effects of LULC change is very crucial in the efficient utilization and management of natural resources. Understanding the trends of LULC change will be very helpful in the land use planning and environment management of a region (Zhao et al. 2013; Li et al. 2018). With the recent developments in geographical information science (GIS) and remote sensing, the researchers can effectively characterize and examine the dynamic changes in LULC (Chaudhuri and Mishra 2016; Tran et al. 2017). The availability of spatiotemporal consistent satellite images and ingenious image processing techniques has improved the efficiency of monitoring these LULC changes.

N. R. Govind (✉) · H. Ramesh
Department of Applied Mechanics & Hydraulics, National
Institute of Technology Karnataka, Surathkal, Mangalore, India
e-mail: nithya_rgovind@yahoo.com

Urbanization is one of the most significant factors that cause LULC change. It is the rise in the population of cities in comparison to the rural population of the region. Urbanization is caused by the transformation of natural land surfaces comprising of vegetation and pervious surface into built-up and impervious surfaces due to the growth in economy and population (Tan et al. 2010; Mathew et al. 2016; Pal and Ziaul 2017). The uncontrolled and unplanned urban growth has led to serious issues on climate and the local environment (Bhat et al. 2017). The rapid urban growth directly or indirectly affects various environmental variables like land cover, temperature, rainfall, and so on. India is facing a high rate of urbanization due to which most of its metropolitan cities are becoming urban jungles. The rapid urbanization in the cities like Mumbai, Delhi, Kolkata, Chennai, and Bengaluru has led to serious environmental issues in the respective regions.

In addition to LULC, land surface temperature (LST) is another imperative parameter which has a significant impact on the environment due to rapid urbanization. The LST patterns give useful information regarding surface physical properties and climate. Assessing the distribution of LST can be helpful in understanding various subjects like evapotranspiration, climate change, and urban climate (Amfield 2003; Bendib et al. 2017). Similar to LULC, LST also has dynamic spatial and temporal variations. LST can be easily obtained from remote sensing data by using the thermal infrared band (Shi and Zhang 2018) at different spatial and temporal scales which gives a better perception of the temperature distribution compared to the in situ observation data. Numerous approaches and algorithms have been proposed by researchers to derive LST from satellite images (Valor and Caselles 1996; Qin et al. 2001; Jiménez-Muñoz and Sobrino 2003; Li et al. 2013). Low and medium spatial resolution spaceborne remote sensing images are usually used for deriving LST from satellite images (Zhou et al. 2014; Liu et al. 2016).

In semiarid regions, a phenomenon of urban cooling effect is experienced due to urbanization. The built-up areas in the semiarid regions experience lesser temperature compared to the surrounding nonurbanized areas. This phenomenon is termed as the urban cool island effect (Frey et al. 2009). Urban cool island effect on the semiarid environment is a very less explored area. Very few researches have been carried out on urban cool island effect, its characterization, and quantification (Rasul et al. 2015, 2017). Several researchers have quantified urban heat island (UHI) and urban cool island

(UCI) in green spaces and water bodies within cities; however, the studies on UCI across a whole urban area are at its infancy and require better apprehensions (Li et al. 2011; Balzter et al. 2017). Research in UCI will provide opportunities for urban planners and policy makers to implement adaptive management strategies toward sustainable cities in an uncertain climate future (Fan et al. 2017).

A lot of studies have been carried out to assess the impact of LULC on LST. LST has been extensively used as a significant parameter in understanding the impacts of LULC change on the environment. Studies on the impact of urbanization on LST in various cities of India like Chennai (Devadas and Rose 2009), Delhi (Ogawa et al. 2012; Babazadeh and Kumar 2015; Grover and Singh 2015), Hyderabad (Franco et al. 2015), Mumbai (Grover and Singh 2015), Nagpur (Kotharkar and Surawar 2015), and Jaipur (Jalan and Sharma 2014) have been carried out by researchers. Most of the cities in India experience a heating effect with the development of urban areas, and the LST increases with the increase in urban area and a decrease in vegetative cover (Chakraborty et al. 2015; Ziaul and Pal 2018). An urban cool island effect is observed in some parts of Central India during the winter season as reported in few studies (Ghosh et al. 2017).

This study aims at analyzing the spatial and temporal distribution of LULC and LST in Bengaluru urban district in the context of urban cool island effect. Assessing the spatial and temporal distribution of LST and LULC in the region is the need of the hour. Previous studies are mainly focused on Greater Bengaluru, which is a small part of the Bengaluru urban district (Ramachandra and Kumar 2009; Ramachandra et al. 2013). None of the studies takes into account the whole of Bengaluru urban district. Considering the district as a whole helps in understanding the spatiotemporal patterns of LULC and LST in a better way as there are agricultural activities by farmers and the urban area is surrounded by barren mountains with shrubs. The urban cool island effect in the study area is also very less explored. Very few studies have been reported on UCI in a semiarid environment. Bengaluru is one of the fast-growing metropolitan cities of India with a semiarid tropical climate. This study focuses on the characterization of UCI based on hot spot analysis which is one of a kind in the study area. The analysis was performed for the time period from 1989 to 2017. The main objectives of this paper are (i) to quantify the land use change

patterns and identify the driving factors, (ii) to explore the spatial and temporal variation of LST, and (iii) to assess the impact of LULC change on LST using hot spot analysis during the time interval 1989–2017. The LULC and LST maps were prepared using multitemporal satellite images.

Study area

The study area selected is Bengaluru urban district in the state of Karnataka, India. Bengaluru is popularly known as the ‘garden city of India’ and the information technology capital of India. It is famous for its cultural heritage and industries encompassing information technology, aerospace, manufacturing, and other sectors. The Bengaluru urban district is geographically located between 77° 34′ 19″ E–12° 59′ 34″ N and 77° 38′ 13″ E–12° 56′ 38″ N, respectively, as shown in Fig. 1. Bengaluru urban district has a geographical area of 2196 km² and is located at an altitude of about 900 m above mean sea level. It is situated midway between the eastern and western coast of the Indian peninsula. The district receives a mean annual total rainfall of 880 mm and has no major rivers. Seasonal dry tropical savanna climate is observed in the district with four seasons, viz., dry season, summer season, south-west monsoon, and retreating monsoon.

At present, Bengaluru has become one of the swiftly growing cities in the world from a tiny village way back in the twelfth century. It has been branded as the ‘Silicon Valley’ of India and is one of the leading technological innovation hubs. According to the Human Development Report (Sudhira et al. 2007), it has a high technological achievement index of 13.

During the decade 2001–2011, Bengaluru urban district recorded a population growth rate of 47.18%. The decadal growth rate increased by 12.10% compared to the previous growth rate. The decadal growth rate of rural areas is 12.16% and that of urban areas is 51.91% which is considerably more than the rate registered in rural areas. The annual rainfall received also exhibits an increasing trend. The extent of urbanization that has occurred in the study area can be acknowledged by the tremendous increase in the population in the past few years. From the year 1970, there has been a steep increase in the population of the region (Fig. 2). Similarly, the plot of annual rainfall exhibits a prominent increase after 1980.

The temperature of Bengaluru has increased by about 2 °C during the period from 1973 to 2007, confirming the phenomenon of urban heat island (Ramachandra and Kumar 2009). From the analysis of monthly temperature and rainfall data from 1901 to 2000, it can be understood that the highest value of the maximum and minimum temperature is recorded in the months of April and May, while the mean rainfall is highest during September and October (Fig. 3). From the analysis of climate variables for the past few decades, it was observed that there is an increase in the minimum, maximum, and average temperature in the region and an increase in the number of rainy days was also spotted during the same time period (Fig. 4). The increase in the amount of precipitation and the rainy days can be attributed to the change in temperature and land use land cover of the region. According to previous studies, there has been a significant change in the land use land cover of the region. Therefore, a detailed study on the spatial and temporal variation of LULC and LST and its interrelationship by considering Bengaluru district as a whole is pertinent at this point in time.

Data and methods

The study is mainly focused on the dry season and employs the Landsat 5 Thematic Mapper (TM) and Landsat 8 Operational Land Imager (OLI) images. Table 1 illustrates the details of the data used in the study. The images were acquired at around 10:00 a.m. Indian Standard Time. The study makes use of various remote sensing methods to estimate the LST and LULC of the study area for the years 1989, 1994, 2001, 2005, 2014, and 2017. The methodology of the study is described in Fig. 5. Survey of India (SoI) toposheet was used for delineation of the study area. Two complimentary softwares were used for the study: ArcGIS10.1 and ERDAS Imagine 14.

LULC mapping

The LULC map of the region was prepared for the years 1989, 1994, 2001, 2005, 2014, and 2017. It was prepared based on supervised classification by employing Maximum likelihood algorithm. Four broad land use classes were identified, namely vegetation, water, barren, and urban (commercial and industrial land,

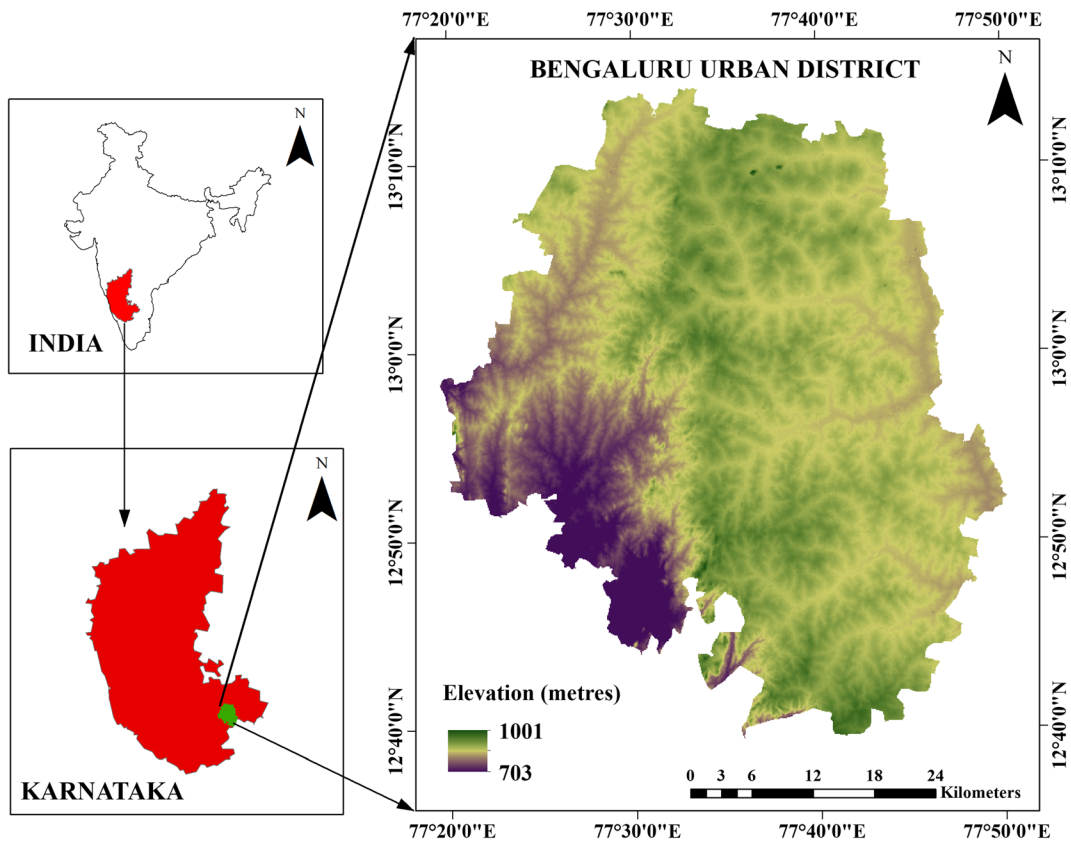


Fig. 1 Location map of the study area

residential area, and impervious surface). The area of each land use class is calculated for comparison.

Accuracy assessment

An unbiased representation of the land cover of a region can be proved by the accuracy of the LULC map. The accuracy of the LULC map is usually measured in terms of a confusion matrix. The rows and columns of the confusion matrix consist of sample points (pixels) allotted to a particular category relative to the actual category

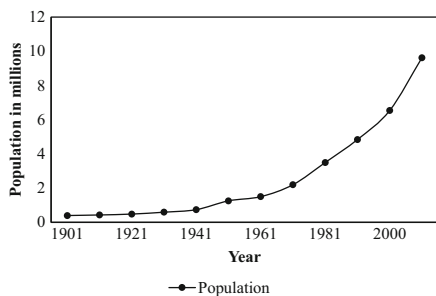


Fig. 2 Distribution of population in the region from 1901 to 2011

as obtained from the ground (Congalton 1991). The rows usually indicate the classified data from satellite images and the columns represent the reference data. The overall accuracy of the map and the accuracy of each class are obtained from the confusion matrix. The overall accuracy is obtained by dividing the total correct units by the total number of units. The individual accuracy is measured using user’s accuracy (error of commission), based on classified data, and producer’s

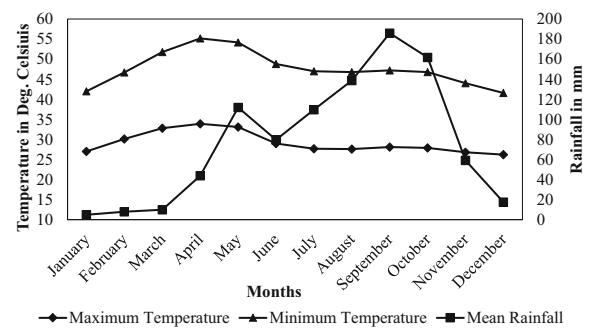
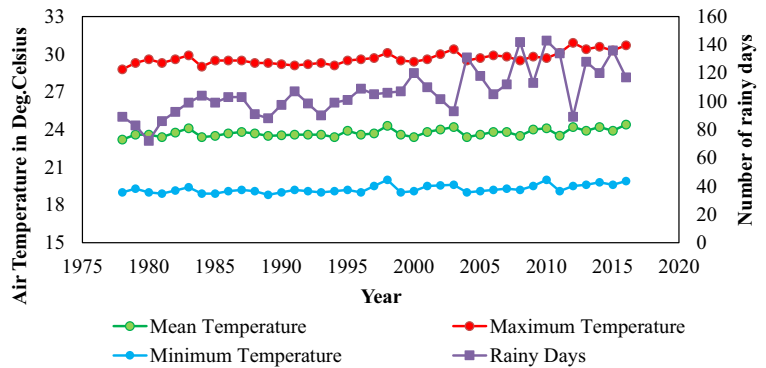


Fig. 3 Variation of monthly mean temperature and rainfall of Bengaluru district based on 1900–2000 data

Fig. 4 Annual temperature variation with number of rainy days in Bengaluru region during 1978 to 2016



accuracy (error of omission), based on reference data (Smits et al. 1999).

Kappa coefficient is another multivariate technique commonly used in accuracy assessment (Cohen 1960). It is used to assess whether the confusion matrix is significantly different from a random result. The kappa analysis can be used to estimate if a classifier result is better than the other by comparing the two metrics (Smits et al. 1999). The kappa coefficient (K) is given by Eq. 1 (Congalton 1991).

$$K = \frac{N \sum_{i=1}^r x_{ii} - \sum_{i=1}^r (x_{i+} \times x_{+i})}{N^2 - \sum_{i=1}^r (x_{i+} \times x_{+i})} \tag{1}$$

Where r is the number of rows in the matrix, x_{ii} is the number of observations in row i and column i , x_{i+} and x_{+i} are the marginal totals of row i and column i ,

respectively, and N is the total number of observations. The value of K ranges from 0 to 1 where 1 represents the complete agreement between the classified and reference data (Pal and Ziaul 2017).

In this study, 230 ground truth points were acquired from Google Earth and from the field using GPS. The overall accuracy, individual accuracies, and kappa coefficient was determined. An overall accuracy higher than 85% indicates the best agreement between the classified and the ground truth data (Foody 2002).

Intensity analysis

Intensity analysis was carried out to analyze the pattern of LULC change. Based on the preliminary studies conducted in the study area, it is observed that major private sector companies particularly information technology at a larger scale were established around the year 2000 which led to the urban growth of Bengaluru. This has tremendously

Table 1 Remote sensing data used in the study

Sensors	Date of acquisition	Path/row	Bands/product used	Resolution (m)	Source
Landsat 5 TM	22 February 1989	144/51	4, 3, 2	30	earthexplorer.usgs.gov
Landsat 5 TM	20 February 1994	144/51	4, 3, 2	30	earthexplorer.usgs.gov
Landsat 5 TM	27 March 2001	144/51	4, 3, 2	30	earthexplorer.usgs.gov
Landsat 5 TM	18 February 2005	144/51	4, 3, 2	30	earthexplorer.usgs.gov
Landsat 8 OLI	15 March 2014	144/51	5, 4, 3	30	earthexplorer.usgs.gov
Landsat 8 OLI	23 March 2017	144/51	5, 4, 3	30	earthexplorer.usgs.gov
MODIS (MYD11A1)	18 February 2005	25/7	LST	1000	ladsweb.nascom.nasa.gov
MODIS (MYD11A1)	15 March 2014	25/7	LST	1000	ladsweb.nascom.nasa.gov
MODIS (MYD11A1)	23 March 2017	25/7	LST	1000	ladsweb.nascom.nasa.gov

*The thermal band is acquired at different resolutions but products were resampled to 30 m pixels by NASA

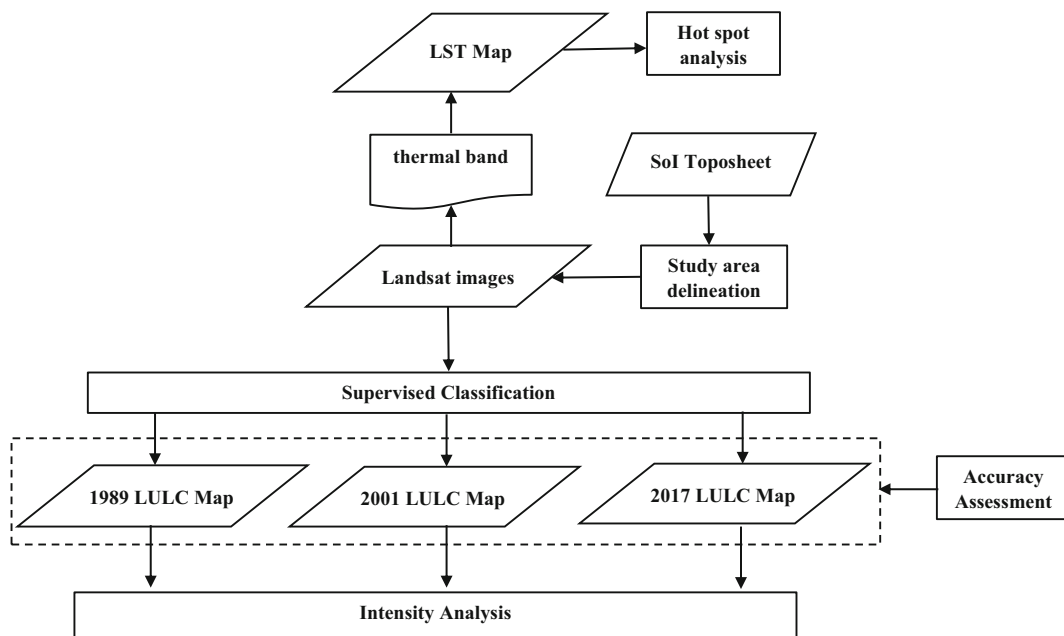


Fig. 5 Flowchart of methodology

increased the housing sector, infrastructural facilities, etc. Therefore, the time period was divided into two intervals from 1989 to 2001 and 2001 to 2017 based on the availability of cloud-free satellite data. The intensity analysis was performed for these two intervals.

The extent and rate of LULC change for the time period in the entire area and in each category are examined using intensity analysis (Aldwaik and Pontius 2012). The intensity analysis can be broken down into three levels, namely interval, category, and transition (Table 2). At the interval level, the variation in the rate of LULC change in the study area was studied by estimating the annual change intensity of each time interval. The intensity analysis is based on the assumption that the annual changes are distributed uniformly across the entire time interval and it is called uniform intensity. The annual change rates obtained are compared with the uniform intensity value. The results from the intensity analysis determined which time interval experienced a faster rate of LULC change compared to the other. In the category level analysis, the intensities of gross gains and gross losses in each LULC class were estimated for both the intervals. The intensity of gain/loss obtained for each class of LULC was then compared with the uniform intensity. In the category level, analysis uniform intensity is the annual change that would occur if the variation within each interval were scattered uniformly across the entire spatial extent. Thus, the dormant and active land use classes and the constancy of their pattern

of change over both time intervals were assessed using category level analysis. At the transition level, the rate of transition from one LULC class to another was analyzed for both the intervals. The observed transitions were compared with the uniform transition intensities to and from land use classes to examine which LULC classes were avoided or targeted in a given time interval (Chaudhuri and Mishra 2016).

In this study, the total time period considered was 28 years (1989–2017) and it was divided into two time intervals: 1989–2001 and 2001–2017. At first, a cross-tabulation matrix is prepared for both the time intervals. Tables 3 and 4 demonstrate the cross-tabulation matrix for the time intervals 1989–2001 and 2001–2017, respectively. The first matrix is obtained by overlaying the LULC map of 1989 and 2001, while the second matrix is obtained by overlaying the maps of 2001 and 2017. The values in the matrices are the area of the corresponding land use class in square kilometers. The total column in the right of the matrix is the area of each class in the initial time, while the total row is the area of each class in the subsequent time. The column in the far right gives the gross losses in each class during the interval, while the row in the bottom gives the gross gains during the interval.

At interval level analysis, the LULC change experienced during both the intervals is analyzed and the time interval in which the land transition is faster is identified.

Table 2 Equations for intensity analysis (Aldwaik and Pontius 2012)

$$S_t = 100\% \times \left(\left\{ \sum_{j=1}^J [(\sum_{i=1}^J C_{ij}) - C_{ij}] \right\} / \left[\sum_{j=1}^J (\sum_{i=1}^J C_{ij}) \right] \right) / (Y_{t+1} - Y_t) \tag{2}$$

$$U = 100\% \times \left(\sum_{t=1}^{T-1} \left\{ \sum_{j=1}^J [(\sum_{i=1}^J C_{ij}) - C_{ij}] \right\} / \left[\sum_{j=1}^J (\sum_{i=1}^J C_{ij}) \right] \right) / (Y_T - Y_1) \tag{3}$$

$$G_{ij} = 100\% \times \left\{ [(\sum_{i=1}^J C_{ij}) - C_{ij}] / (Y_{t+1} - Y_t) \right\} / \sum_{i=1}^J C_{ij} \tag{4}$$

$$L_{ii} = 100\% \times \left\{ \left[\left(\sum_{j=1}^J C_{ij} \right) - C_{ii} \right] / (Y_{t+1} - Y_t) \right\} / \sum_{j=1}^J C_{ij} \tag{5}$$

$$R_{in} = 100\% \times [C_{in} / (Y_{t+1} - Y_t)] / \sum_{j=1}^J C_{ij} \tag{6}$$

$$W_m = 100\% \times \left\{ [(\sum_{i=1}^J C_{im}) - C_{im}] / (Y_{t+1} - Y_t) \right\} / \sum_{j=1}^J [(\sum_{i=1}^J C_{ij}) - C_{im}] \tag{7}$$

$$Q_{mj} = 100\% \times [C_{mj} / (Y_{t+1} - Y_t)] / \sum_{j=1}^J C_{ij} \tag{8}$$

$$V_m = 100\% \times \left\{ [(\sum_{i=1}^J C_{mj}) - C_{im}] / (Y_{t+1} - Y_t) \right\} / \sum_{j=1}^J [(\sum_{i=1}^J C_{ij}) - C_{im}] \tag{9}$$

Where J = number of classes; i = index of a class at the initial time point for a particular time interval; j = index for a class at the final time point; m = index for the losing class in the transition of interest; n = index for the gaining class in the transition of interest; T = number of time points; t = index for the initial time point of interval (Y_t, Y_{t+1}) , where t ranges from 1 to $T - 1$; Y_t = year at time point t ; C_{ij} = number of pixels that transition from class i at time Y_t to class j at time Y_{t+1} ; S_t = annual intensity of change for time interval (Y_t, Y_{t+1}) ; U = value of uniform line for time intensity analysis; G_{ij} = annual intensity of gross gain of class j for time interval (Y_t, Y_{t+1}) ; L_{ii} = annual intensity of gross loss of class i for time interval (Y_t, Y_{t+1}) ; R_{in} = annual intensity of transition from class i to class n during the time interval (Y_t, Y_{t+1}) where $i \neq n$; W_m = value of uniform intensity of transition to category n from all non- n classes at time Y_t during the time interval (Y_t, Y_{t+1}) ; Q_{mj} = annual intensity of transition from class m to class j during the time interval (Y_t, Y_{t+1}) , where $j \neq m$; and V_m = value of uniform intensity of transition from class m to all non- m classes at time Y_{t+1} during the time interval (Y_t, Y_{t+1})

At the category level, the four different categories, namely vegetation, water, urban, and barren, were examined, and the active and dormant categories were determined. In the transition level, the analysis was carried out in two sublevels: firstly, the rate of transition from urban to other classes, and secondly, the rate of transition from vegetation to other classes were determined in both the time intervals. The LULC class which is intensively avoided or targeted is identified in this level of analysis.

LST retrieval

Land surface temperature of the study area was retrieved from the thermal infrared band of Landsat images. The approach used in this study for LST retrieval is a simple single-channel algorithm which can be employed for coarse resolution images. The method incorporates atmospheric profile values and emissivity obtained from NDVI, thereby improving the accuracy of the extraction. Since the time period considered for the study is from 1989 to 2017 and the dataset used is Landsat data, an LST extraction method which can be applied to sensors with single

thermal band data was adapted for the study. The conversion of pixel data of the Landsat images to LST comprises of the following steps (Landsat, N.A.S.A. (7) 2011; Landsat, N.A.S.A. (8) 2015):

1. Conversion of pixel values to spectral radiance (Landsat 5 TM)

$$L_\lambda = G_{\text{rescaled}} \times Q_{\text{Cal}} + B_{\text{rescaled}} \tag{10}$$

In the case of Landsat 8,

$$L_\lambda = M_L \times Q_{\text{Cal}} + \Delta_L \tag{11}$$

Where L_λ is the spectral at-sensor radiance, G_{rescaled} is the rescaled gain, B_{rescaled} is the rescaled bias, Q_{Cal} is the quantized calibrated pixel value, M_L is the radiance multiplicative scaling factor for the band, and Δ_L is the radiance additive scaling factor for the band.

In the case of Landsat ETM+ and Landsat 8 images, atmospheric corrections are applied to the spectral radiance obtained, while for Landsat 5 TM, the spectral

Table 3 Land transition matrix of the study area for the time interval 1989–2001 (km²)

	Category	2001				Total	Gross loss
		Vegetation	Water	Urban	Barren		
1989	Vegetation	417.31	9.87	120.16	281.09	828.43	411.12
	Water	24.62	17.37	7.23	8.59	57.82	40.44
	Urban	10.38	0.51	75.44	9.64	95.97	20.53
	Barren	191.66	1.31	212.16	813.61	1218.74	405.13
	Total	643.97	29.06	414.98	1112.94		
	Gross gain	226.66	11.69	339.54	299.33		

radiance is directly converted to LST in Kelvin (due to the absence of atmospheric corrections values).

- Application of atmospheric corrections values to spectral radiance for Landsat 7 ETM+ and Landsat 8 images (McCarville et al. 2011; Tran et al. 2017)

$$L_T = L_\lambda - L_u - \tau(1 - \varepsilon)L_d / (\tau \times \varepsilon) \quad (12)$$

Where L_T is the surface leaving radiance, L_u is the upwelling radiance, L_d is the downwelling radiance, τ is the atmospheric transmission, and ε is the surface emissivity.

The values of L_u , L_d , and τ were evaluated using the Atmospheric Correction Parameter Calculator online tool (<http://atmcorr.gsfc.nasa.gov>; viewed on January 2018). The surface emissivity was estimated based on the normalized difference vegetation index (NDVI) threshold method introduced by Valor and Caselles (1996). The method uses the green coverage ratio and NDVI for the assessment of surface emissivity (Shi and Zhang 2018).

- Conversion of spectral radiance to LST

$$T = K_2 / [\ln(K_1 / L_T + 1)] \quad (13)$$

Where L_T is the surface leaving radiance in watts/(m² ster μ m) (for Landsat 5 TM image, $L_T = L_\lambda$); K_1 , K_2 are the calibration constants of Landsat images (K_1 in watts/(m² ster μ m) and K_2 in Kelvin); and T is the surface temperature in Kelvin.

The LST maps obtained were validated using MODIS LST data; 100 random sample points were selected from extracted LST maps and MODIS data for each year, and a scatterplot was created to determine the coefficient of correlation (Bendib et al. 2017). The value of correlation coefficient indicates the accuracy of the LST map prepared.

Hot spot analysis

The spatial correlation of LST in the study area was examined by employing the optimized hot spot analysis tool (Getis–Ord G_i^*) in the ArcGIS software. The optimized hot spot analysis tool interrogates your data to

Table 4 Land transition matrix of the study area for the time interval 2001–2017 (km²)

	Category	2017				Total	Gross loss
		Vegetation	Water	Urban	Barren		
2001	Vegetation	203.06	11.44	231.57	190.53	636.60	433.54
	Water	8.57	9.34	5.45	5.41	28.77	19.44
	Urban	48.32	0.58	267.86	97.53	414.29	146.43
	Barren	87.21	0.82	446.47	574.73	1109.22	534.49
	Total	347.16	22.18	951.35	868.20		
	Gross gain	144.10	12.84	683.50	293.47		

obtain the settings that will yield optimal hot spot results. The presence of hot spots and cold spots over the entire area was characterized by comparing each feature (LST value) with its neighboring features (Ord and Getis 1995). Comparing the value of a given feature with its neighboring features is important in the characterization of the spatial relationship of features (Nelson and Boots 2008). Hot spots are regions where the maximum value of the feature is clustered, while cold spots are regions where the minimum value of the feature is clustered. A feature with a high value should be bounded by other features with high value then it becomes a statistically significant hot spot. The quantification and characterization of spatial autocorrelation of remotely sensed imagery can be effectively carried out by this technique, the spatial dependence for each pixel is measured, and the relative magnitude of the digital numbers in the neighborhood of the pixel is indicated. The Getis–Ord G_i^* local statistics is calculated using (ESRI 2017)

$$G_i^* = \frac{\sum_{j=1}^n w_{i,j} x_j - \bar{X} \sum_{j=1}^n w_{i,j}}{\sqrt{s \left(n \sum_{j=1}^n w_{i,j}^2 - \left(\sum_{j=1}^n w_{i,j} \right)^2 \right)}} \quad (14)$$

Where x_j is the attribute value of the feature j , w_{ij} is the spatial weight between features i and j , n is the total number of features and

$$\bar{X} = \frac{\sum_{j=1}^n x_j}{n} \quad (15)$$

and

$$S = \sqrt{\frac{\sum_{j=1}^n x_j^2}{n} - \bar{X}^2} \quad (16)$$

The G_i^* statistic value obtained for each feature in the dataset is a z-score. Clustering of high values results in higher positive z-scores (hot spot), and clustering of smaller values results in smaller negative z-scores (cold spot). The statistical significance of clustering for a specified distance is indicated by a z-score value (99% significant: > 2.58 or < -2.58 ; 95% significant: > 1.96 or < -1.96 ; 90% significant: > 1.65 or < -1.65). To be statistically significant, at a significance level of 0.01(99%), a z-score would have to be less than -2.56

or greater than 2.56. Seven categories were identified from the statistical results: very cold spot, cold spot, cool spot, not statistically significant, warm spot, hot spot, and very hot spot. The LST pattern was linked with the change in LULC to assess the impact of LULC change on LST. This methodology gives a better insight into the impact of LULC change rather than concentrating on certain high and low LST values only. The hot spot maps were created for three years 1989, 2001, and 2017.

Pearson’s correlation coefficient

Pearson’s correlation coefficient is introduced in this study to establish the relationship between LST and LULC classes. It is the measure of the degree of linear correlation between two variables and is determined by the value of r (Zhang et al. 2019). It is a dimensionless measure, and the value ranges from -1 to $+1$ where -1 indicates the variables have a perfect negative correlation, $+1$ indicates the variables have perfect positive correlation, whereas 0 indicates there is no linear relationship between the two variables. Pearson’s correlation coefficient r between two variables X and Y is given by Eq. 17 (Asuero et al. 2006)

$$r = \frac{\sum_{i=1}^n (X_i - \bar{X})(Y_i - \bar{Y})}{\sqrt{\sum_{i=1}^n (X_i - \bar{X})^2} \sqrt{\sum_{i=1}^n (Y_i - \bar{Y})^2}} \quad (17)$$

Where \bar{X} and \bar{Y} are the mean of the variables X and Y , respectively, and n is the sample size.

Results

The LULC and LST maps were prepared for the years 1989, 1991, 2001, 2005, 2014, and 2017. The spatial and temporal patterns of LULC and LST were analyzed using intensity analysis and hot spot analysis, respectively. The results prove that there is a significant change in land cover and LST of the region over the years.

LULC classification

The two main classes observed from LULC classification are urban and barren land. Water constitutes only a very small portion of the study area. The accuracy of the land use map obtained was determined by comparing

the ground truth measurements with the classified data. The overall accuracy of the LULC maps obtained for the different years (1994, 2001, 2005, 2014, and 2017) ranges from 84 to 91% and the kappa coefficient ranges from 0.85 to 0.91. For recent years, the overall accuracy of the LULC map is better compared to the earlier years since the spatial resolution of the recent images was improved using the pan-sharpening technique. The values of overall accuracy and kappa coefficient suggest that the classified map and the reference data have good agreement with one another.

The results of the LULC classification show that there is a significant change in LULC of the region from 1989 to 2017 (Fig. 6). The urban area has increased from 4 to 43% during the period from 1989 to 2017, while the vegetation has decreased from 38 to 16% and barren land has decreased from 55 to 40% of the total area. The LULC change for the period from 1989 to 2017 is analyzed by means of intensity analysis. For the past 28 years, the urban area has increased by about 40%, while the other land use classes like vegetation, water, and barren have decreased. This was mainly due to the increase in information technology establishments which in turn accelerate real estate and infrastructural projects at a faster rate to cater to housing and other services. The two intervals considered for analysis are 1989–2001 and 2001–2017.

Intensity analysis of LULC change

Figure 7 illustrates the time interval analysis for the two intervals. The bars that extend to the right side display the intensity of an annual area of change within each time interval, and the bars to the left indicate the gross area of total changes in each interval. The left-hand side of the figure shows that the change in area in the region during the second interval (2001–2017) is more and the reason of it being the duration of the first interval is larger than the duration of the second time interval. Analyzing the right-hand side of the figure, it is observed that the annual change in area is more prominent in the interval 1989–2001. This is obtained from the value of uniform intensity. The uniform line is the vertical line drawn along the right side of the figure. The bars that extend beyond the uniform line indicate that the change is faster in that interval. In this case, the annual change in the area during the time interval 1989–2001 is faster, while it is slower in the interval 2001–2017. This indicates that the LULC change is faster in

the interval 1989–2001, while it is slower during 2001–2017. After analyzing the rate of LULC change of each interval, category level analysis for each interval is carried out. This is due to the fact that many multinational IT companies have started their operation during 1989–2001.

Figures 8 and 9 illustrate the category level analysis for the intervals 1989–2001 and 2001–2017, respectively. The bars that spread to the right side indicate the intensity of annual gains and losses within each category and those to the left side display gross annual area of gains and losses in the study area. From the left side of Fig. 8, it is clear that the urban area has the largest gain during the interval while vegetation has the largest loss. In the case of Fig. 9, the largest gain is for the urban area, but the largest loss is shifted to barren land. Hence, the behavior of urban area is similar in both intervals. The active and dormant classes can be identified by the uniform line drawn in the right side of the figure. For the interval 1989–2001, the urban, vegetation, and water are the active land use classes, while barren land is dormant during the interval. Among the active land use classes, the urban area has experienced significant gain, while vegetation and water experienced a significant loss. A similar behavior is observed for the interval 2001–2017 also where the urban, vegetation, and water are the active classes and barren land is the dormant class. The study region exhibits a similar behavior for the category level analysis in both intervals.

Figure 10 shows the transition intensity analysis to urban for the time interval 1989–2001. Figure 11 shows the transition intensity analysis to urban for the time interval 2001–2017. The bars that spread to the left side imply a gross annual area of transitions to urban, and the bars to the right side imply the intensity of annual transitions to urban within each nonurban category. The transition to urban from other nonurban classes is analyzed. From the left side of Fig. 10, it is observed that the major transition to the urban area has occurred from the barren land. The area of transition from barren to urban is more compared to the other two classes. A similar behavior is observed for the second interval also proving that the transition from barren to urban is stationary. The uniform line on the right side of the figure determines whether the transition should be avoided or targeted. Since the barren land extends beyond the uniform line, it should be targeted. The transition from barren to urban land is prominent compared to the other nonurban classes. The transition from water and

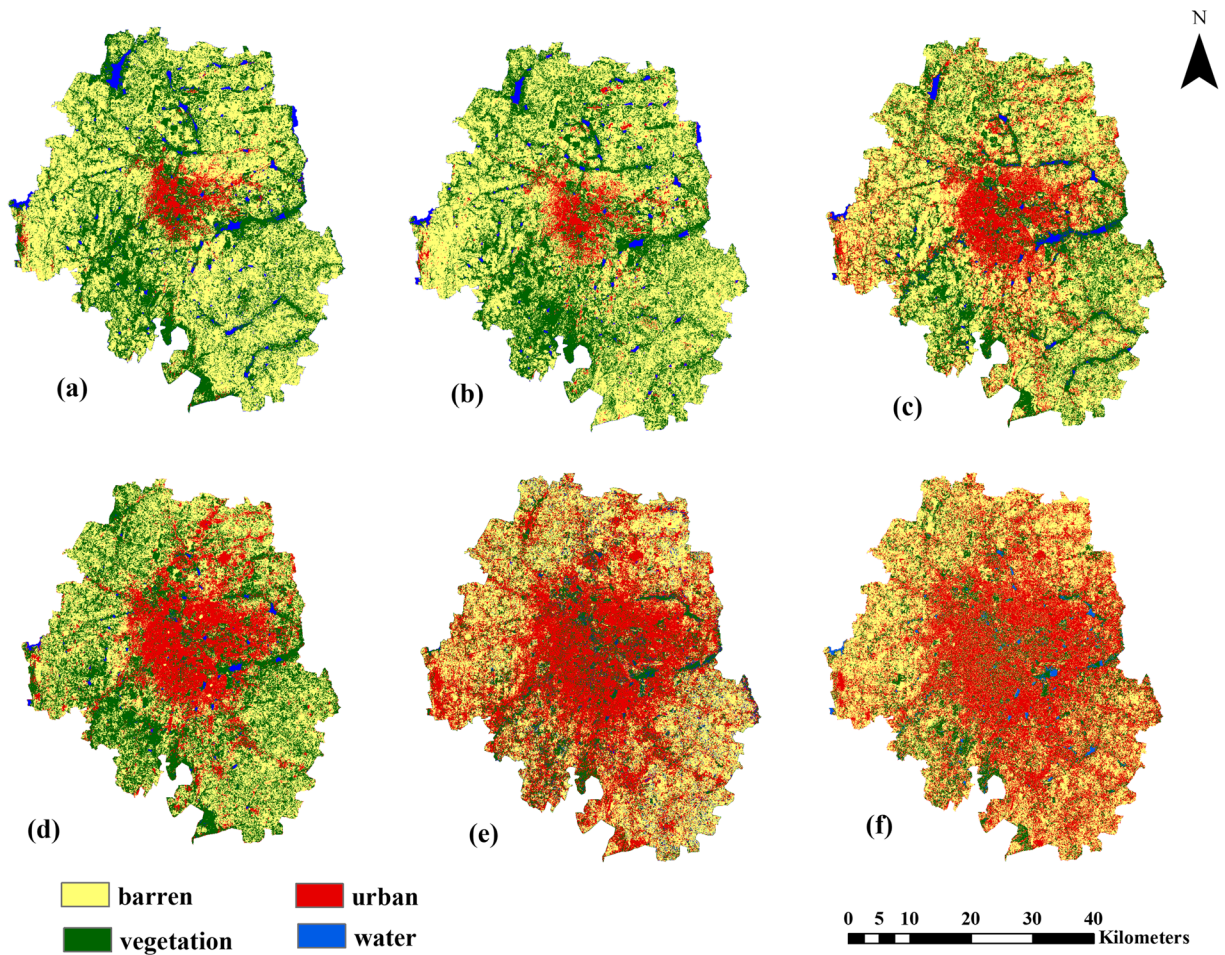


Fig. 6 LULC map of the study area for the years **a** 1989, **b** 1994, **c** 2001, **d** 2005, **e** 2014, and **f** 2017

vegetation can be avoided, and the transition from barren land to urban should be focused. Figure 11 also exhibits a similar behavior where the major transition to the urban area has occurred from barren land. Thus,

the transition from barren to urban is stationary according to the intensity analysis.

The transition intensity analyses from vegetation for the time intervals 1989–2001 and 2001–2017 are shown

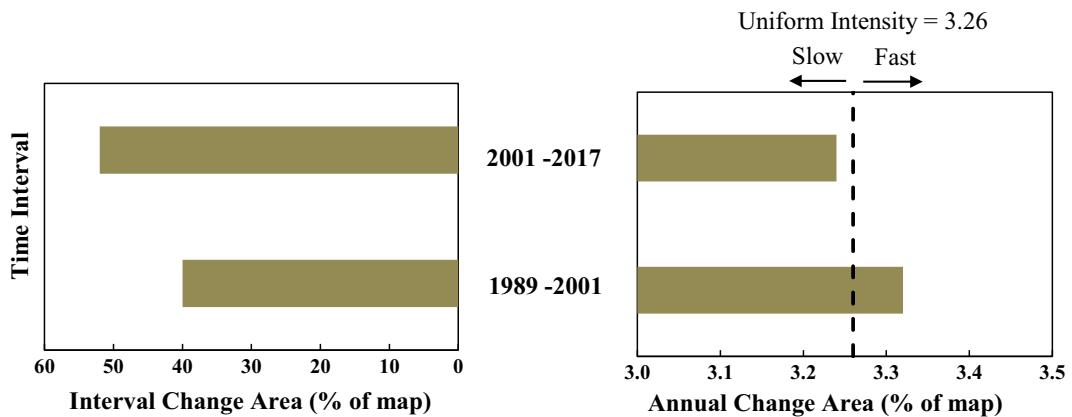


Fig. 7 Time intensity analysis for two time intervals: 1989–2001 and 2001–2017

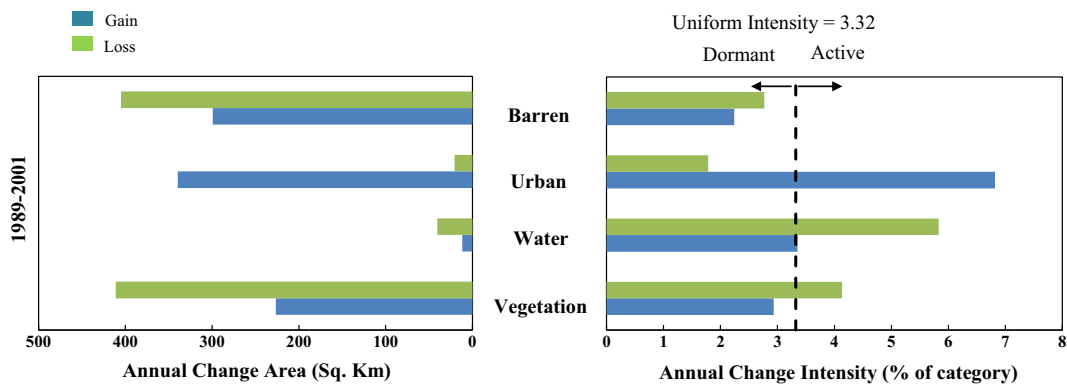


Fig. 8 Category intensity analysis for the interval 1989–2001

in Figs. 12 and 13, respectively. The left side portion of the figure indicates the gross annual area of transitions from vegetation and the right side indicates the intensity of annual transitions from vegetation within each nonvegetation category. From the left side of Fig. 12, it can be observed that the area of transition from vegetation to barren is more compared to urban and water. In the second interval (Fig. 13), the largest transition from vegetation to barren was noticed, while the transition from vegetation to urban is decreased and that of water has increased compared to the first interval. The vertical uniform line to the right side of the figure determines as to whether the transition is targeted or avoided. In both the time intervals, the transition intensity from vegetation to urban and water is more. These two transitions are targeted, while in the second interval, the transition intensity to urban is less compared to the previous interval.

Concisely, it can be said that the major change in land use has occurred during the period of 1989 to 2001 compared to the other interval considered. There is a major increase in the urban area in both the intervals.

The vegetation and water have undergone a major loss in both the intervals with vegetation experiencing a higher loss in the second interval compared to the first. In both the intervals, it is seen that the transition from barren to urban is intensely targeted and the transition from vegetation to water is also targeted.

Spatiotemporal variation of LST

The LST patterns of the study area for the years 1989, 1994, 2001, 2005, 2014, and 2017 are shown in Fig. 14. The LST obtained was validated using the MODIS-derived LST. The MODIS data used is MYD11A1 with a spatial resolution of 1 km. The spatial resolution of the LST retrieved from Landsat images was aggregated to 1 km for comparison. A significant positive correlation between the LST estimated from Landsat data and MODIS-derived LST was obtained from the scatter plot with 100 random sample points. Correlation coefficients in the range of 0.70 to 0.74 were obtained for different years. This shows the accuracy and reliability of the method used for LST retrieval. There is a substantial

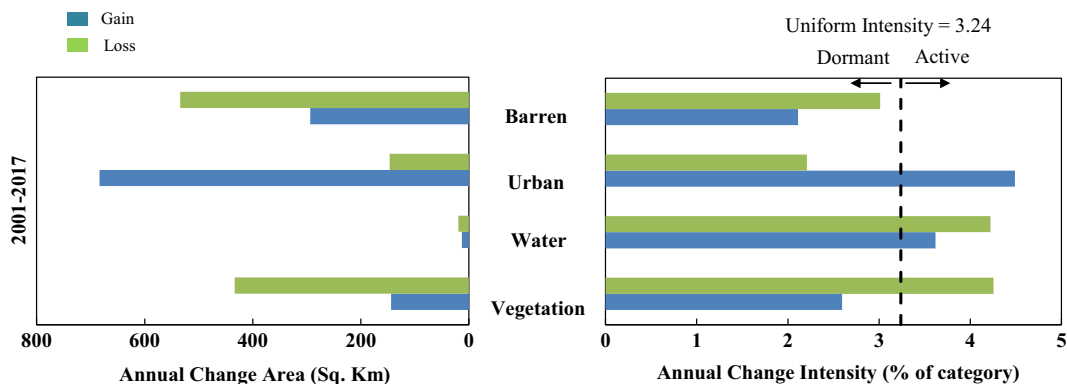


Fig. 9 Category intensity analysis for the interval 2001–2017

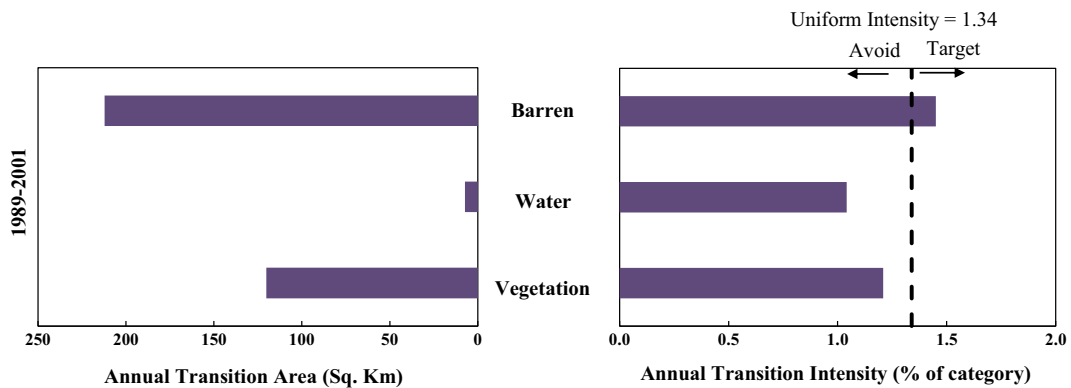


Fig. 10 Transition intensity analysis to urban for the interval 1989–2001

increase in the LST of the region from 1989 to 2017. In can be observed that the maximum, minimum, and mean LST of the region have increased during the period from 1989 to 2017.

The variation of LST in the study area for the years 1989, 2001, and 2017 were plotted in Fig. 15 and examined for understanding the change in LST patterns. In the year 1989, 53% of the study area was under the LST range of 32 to 38 °C and 45% experiences an LST range of 26 to 32 °C. In the year 2001, 72% of the study area experiences an LST of 38 to 44 °C and 16% experiences an LST of 32 to 38 °C. For the year 2017, 68% of the study area experiences an LST of 38 to 44 °C and 27% experiences an LST of 32 to 38 °C. Thus, it is evident that there is a clear shift in the range of LST in the region from 1989 to 2017. In the year 1989, only a small percentage of the study area experiences an LST of 38 to 44 °C, whereas in 2017, 68% of the area falls into this category. Over the years from 1989 to 2017, the mean LST has increased by about 7 °C.

On analyzing the pattern of LST for a particular year, it is observed that the lowest values of LST were traced toward the center portion of the study area while the higher values were observed along the periphery of the study area. The center part of the study area is cooler compared to the surrounding area. This was mainly due to the presence of large biological and recreational parks of size more than 300 acres with lots of trees, lawns, and water bodies as observed in the LULC map.

Apart from this, the LST derived from the satellite images was compared with the air temperature of the region. The maximum, minimum, and mean values of LST and the air temperature were compared for the different years. A comparatively higher correlation was obtained for maximum temperature with a correlation coefficient of greater than 0.81, while 0.80 was obtained for minimum temperature. The reason for the same is that the minimum air temperature is usually measured during the night while the minimum LST is the minimum temperature observed at the time of acquisition of the satellite image.

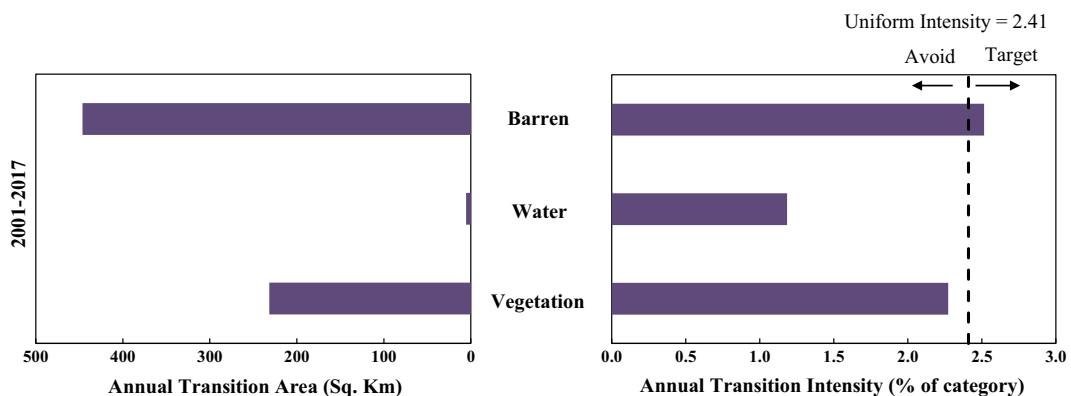


Fig. 11 Transition intensity analysis to urban for the interval 2001–2017

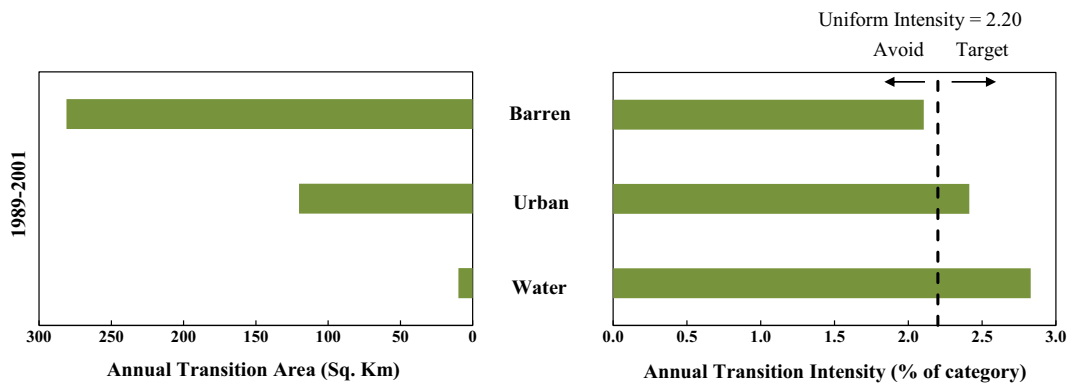


Fig. 12 Transition intensity analysis from vegetation for the interval 1989–2001

LST and LULC relationship

The mean LST of each land use type is estimated for the years 1989, 1994, 2001, 2005, 2014, and 2017. Table 5 demonstrates the change in the distribution of LST for different classes for the years 1989, 2001, and 2017. There is a sizeable increase in the mean LST for each land use type. During the period from 1989 to 2017, the mean LST of vegetation has increased by about 7 °C, the LST of water increased by 6 °C, and the LST of urban and barren land by 8 °C. Meanwhile, there are an increase in the urban land and a considerable decrease in the area of vegetation, water, and barren land. The change in LST has occurred mainly during the period from 1989 to 2001. This was justified through the intensity analysis that the change is faster during this period (1989–2001). The highest increase in LST is observed for built-up and barren land. The vegetation class in the study area mostly consists of urban vegetation, i.e., residential lawns, trees, shrubs, and grasses along the paved surfaces. Due to this, some pixels (spatial resolution of 30 m) will have a mixed land cover type, and in the supervised classification with maximum likelihood

algorithm, a mixed pixel is classified into a particular class based on the proportion of the class. Hence, vegetation class exhibits a relatively equal increase in LST with urban in this study. Even though there is an increase in the LST of the region, lower LST values are observed toward the center where the urban area is concentrated, and higher values are observed along the periphery where barren land is accumulated. This might be due to the presence of several parks and water tanks situated in the area.

There exists a prominent impact of LULC change on the LST of the study region. The urban area has increased by approximately 40% of the total area, and the mean LST has increased by about 8 °C (for urban) from 1989 to 2017. Overall, the study shows a positive correlation between urban land and LST over the area. However, the increase in LST can be attributed to the rise in the impervious area of the region with modern buildings and construction materials at large and usage of HVAC, vehicular pollution, etc. on a lighter scale which could be investigated separately.

The LST for the different LULC classes for the period of interest was compared using the Pearson

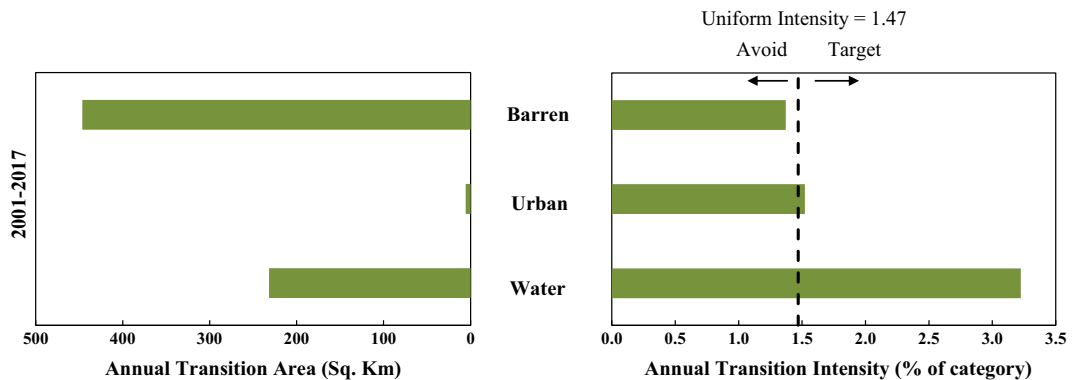


Fig. 13 Transition intensity analysis from vegetation for the interval 2001–2017

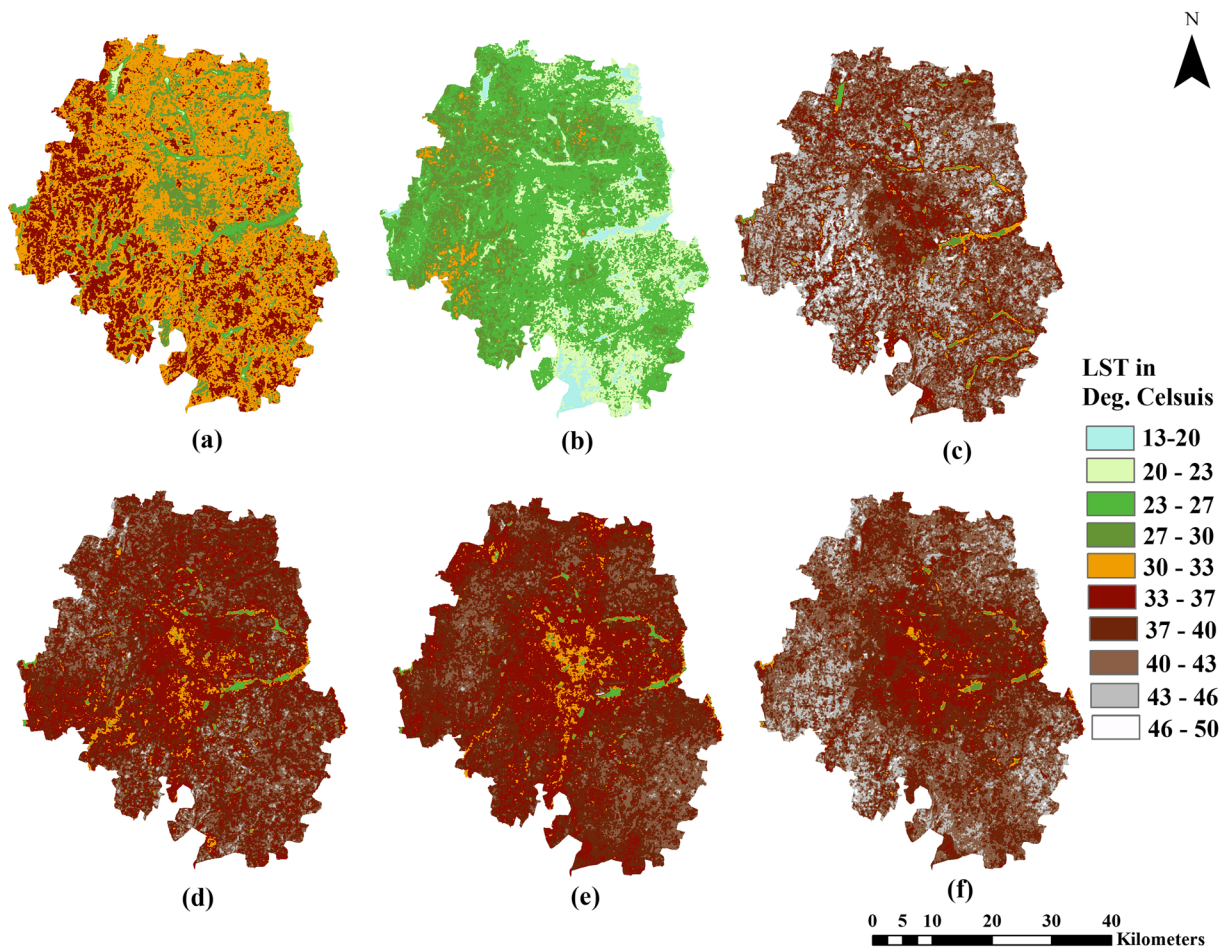


Fig. 14 LST Map of the study area for the years **a** 1989, **b** 1994, **c** 2001, **d** 2005, **e** 2014, and **f** 2017

correlation coefficient. Figure 16 illustrates the interrelation between mean LST of the four land use classes for the years 1989, 1994, 2001, 2005, 2014, and 2017. The correlation coefficients obtained for the classes vegetation, water, barren, and urban are 0.77, 0.88, 0.76, and 0.74, respectively. A relatively high value of correlation

coefficient (greater than 0.6) indicates that there is a linear relationship between the LST of the different LULC classes with time. There is a gradually increasing trend noticed in the mean LST of the LULC classes. One of the limitations of this study is that only six images were used for determining the correlation coefficient due to which an exact picture cannot be established.

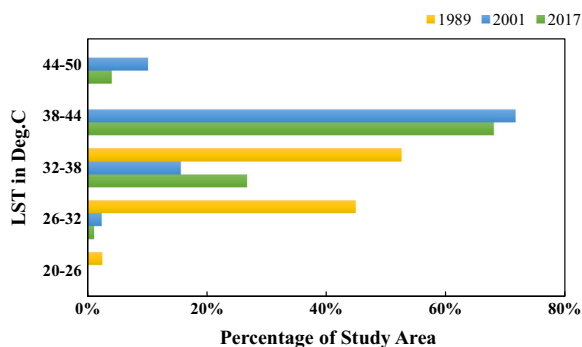


Fig. 15 The variation of LST in the study area

Impact of LULC on LST

Hot spot identification using Getis–Ord G_i^* statistics is widely used in various research areas like natural disaster estimation (Harris et al. 2017), crime analysis (Craglia et al. 2000), road accident evaluation (Prasannakumar et al. 2011), and heat vulnerability assessment (Wolf and McGregor 2013). In this study, the impact of LULC change on LST was examined using this method. The hot spot map of Bengaluru was created for three different

Table 5 Mean LST and land use area of the study region

Land use types	1989		2001		2017		Change during 2001–1989		Change during 2017–2001	
	Mean LST (°C)	Area (km ²)	Mean LST (°C)	Area (km ²)	Mean LST (°C)	Area (km ²)	LST (°C)	% of area	LST (°C)	% of area
Vegetation	29.74	829.54	37.00	644.83	36.93	347.16	7.26	8.38	0.07	13.4
Water	24.90	57.89	29.07	29.1	31.06	22.18	4.17	1.31	1.99	0.31
Barren	31.58	1220.4	41.23	1114.4	40.06	862.3	9.65	4.81	1.17	10.91
Urban	29.43	96.09	39.18	415.53	37.94	951.71	9.75	14.49	1.24	24.62

dates (Fig. 17). This provides a better understanding of the LST distribution in the area. The identification of hot spot and cold spot by this method does not depend on a single high or low LST value and, hence, provides a better picture of the hot and cold regions.

The cold spots are mainly clustered in and around the water bodies, and the hot spots are clustered in the barren land. It is observed that over time, some “not significant” regions have become cold spot and it is indicated by the transformation of certain parks and water tanks in the center part of the study area to cold spots. On the whole, hot spot regions are more compared to cold spot regions. Approximately 24% of the study area is warmer, while 14% is cooler throughout the time period. The hottest land use type is barren, and the coldest land use type is water.

During the time period, hot spots have a tendency to decrease (39.56% in 1989 to 35.04% in 2017), while the cold spots tend to increase (14.36% in 1989 to 22.89% in 2017). In the years 1989 and 2001, water body contributed to more than 50% of the cold spots, while in 2017, the cold spots are mainly observed in the urban area. Over the time period, a localization of cold spots is observed in the center part of the Bengaluru where the major land use type is

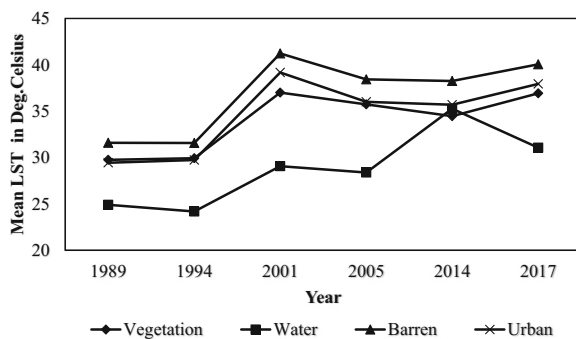
urban. At the same time, hot spots are observed in the peripheral regions of Bengaluru where the major land use type is barren land. As urban expansion occurs, the cold spots are clustered in the urban area. Hence, it can be inferred that in recent years, the urban area has become cooler than the surrounding rural area confirming the existence of an urban cool island in Bengaluru. Urban cool islands are regions where the urban area is cooler than the surrounding rural area.

Discussion

The proposed research deals with LULC change and its impact on surface heating patterns for the metropolitan city of Bengaluru. Monitoring and prediction of LULC change and its impact on the environment is a topic of growing interest in the present scenario.

The main objectives of this study were to assess the spatiotemporal patterns of LULC and LST and to explore the impact of LULC on LST for the period from 1989 to 2017. Intensity analysis was employed to analyze the variations of LULC and its driving forces, and the patterns of LST were investigated by employing hot spot analysis. This research can be replicated for other cities experiencing a significant change in land cover due to urbanization over the years.

The results show that Bengaluru has experienced a significant increase in the urban area during the period from 1989 to 2017. During the period from 1989 to 2000, the rate of land use change is faster compared to the interval 2001 to 2017, and the transition exhibited is from barren to urban. Over the period of 28 years, LST has increased by about 6 °C and the mean LST of the urban area increased by almost 8 °C. Another significant

**Fig. 16** Variation of mean LST for different land use classes

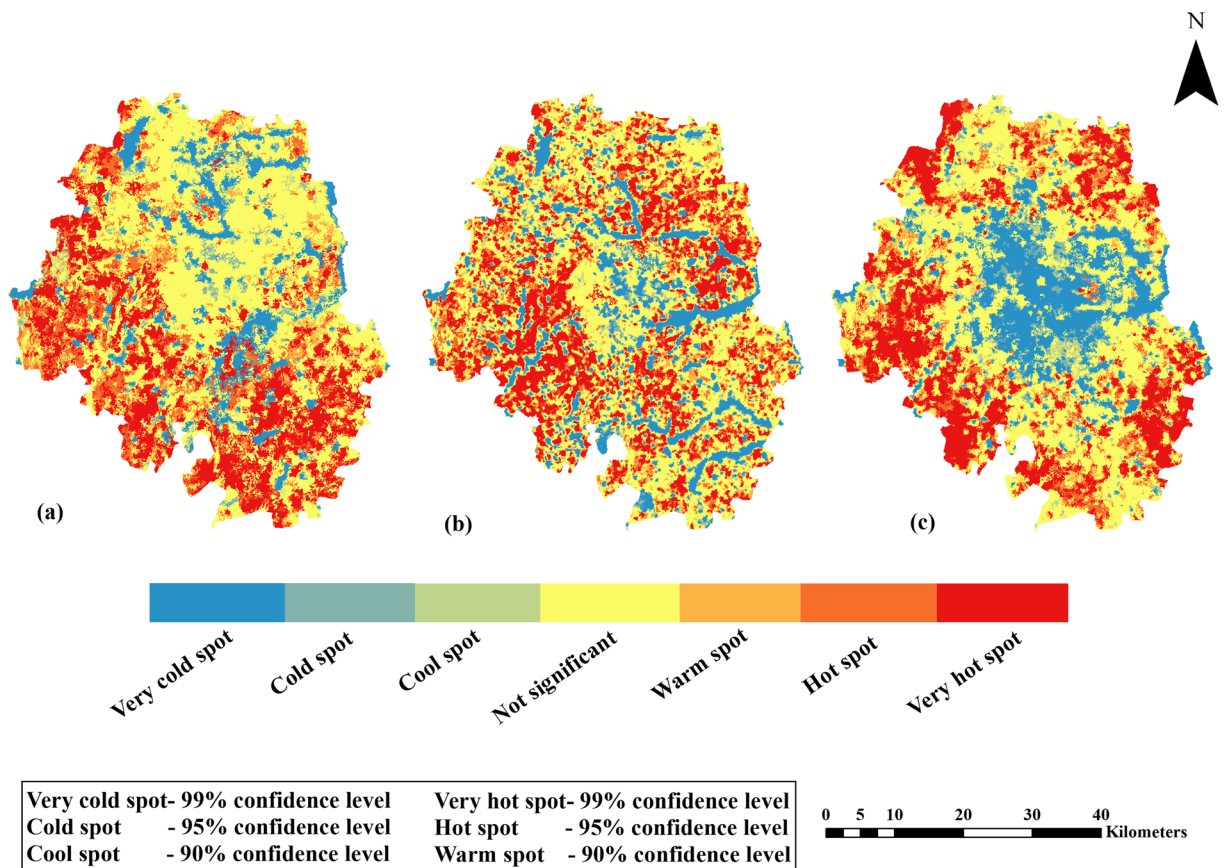


Fig. 17 Hot spot map of study area for the years a 1989, b 2001, and c 2017

observation from the study is that the cold spots have increased and it is mainly clustered in the urban area.

The findings of this research can be attributed to the urbanization experienced by the study area during the past years. Numerous public sector and private sector companies were established after the year 1990 which led to the migration of people from different parts of the country to Bengaluru. The urban growth that commenced in the 1990s is still advancing in the region with the drastic increase in population and urban area. Due to urbanization, the impervious area has increased which in turn led to the surface heating effect in the area. The daytime urban cool effect can be ascribed to different factors. Bengaluru urban district constitutes several parks like Cubbon Park and Lalbagh Botanical Garden which are the two major spots and has several water tanks and lakes which affect the LST of the region. The daytime LST pattern of the area is due to the intense heat waves produced in the nonurban area during the summer season. In the summer season, the evapotranspiration in the outskirts of the city will be very less due to

low vegetation. At the same time, the evapotranspiration in the urban areas will be high due to human population, planted trees, and gardens leading to a cooling effect in the urban area compared to the surrounding (Ghosh et al. 2017).

The urban growth and surface warming effect of Bengaluru obtained from this study is in unison with the previous studies (Ramachandra and Kumar 2009; Ramachandra et al. 2013) reported in the region. However, the urban cool effect in Bengaluru is not reported in any of the previous literatures as most of the studies were focused on the urban core termed as Greater Bengaluru. Studies carried out in other major Indian cities are mainly focused on the urban heating patterns and its adverse effects on the human community by employing different methodologies. Grover and Singh (2015) reported that urban heating effect in Delhi is observed to be less prominent due to the mixed land use type and vegetation cover. The LST pattern exhibits a negative correlation with vegetation and a positive correlation with built-up in Indian cities like Chennai (Faris and

Reddy 2010) and Nagpur (Kotharkar and Surawar 2015), while the temperature profile experiences a dip in areas with water bodies, lakes, and parks as reported in Hyderabad (Franco et al. 2015).

Conclusion

The study presents a comprehensive approach for analyzing the spatiotemporal variation of LULC and LST and the impacts of LULC change on the environment. The LULC change pattern is analyzed using intensity analysis, and the impact of LULC on LST is quantified using hot spot analysis. Significant changes in the LULC and LST pattern have been observed in the study area from 1989 to 2017. The LULC change during the period from 1989 to 2001 is faster compared to the period from 2001 to 2017. The major change witnessed by the study area during this period is the increase in urban which is due to the transition from vegetation and barren to urban. The vegetative cover in the area is extensively affected during this transition. The growth of the urban region has been from center to outwards. The LST pattern of the region has also changed during the study period. The mean LST of the study area has increased overall by 6 °C during the period from 1989 to 2017. Over the years, there has been a shift in the range of maximum LST (experienced by more than 50% of the area).

This change in LST can be attributed to the increased urban area of the region by the addition of a greater number of information technology companies. The impervious area has increased drastically from 1989 to 2017. In the past 30 years, the study area has undergone large urban land use changes, and one of the main reasons for this is the IT revolution in the region. Bengaluru has witnessed a tremendous increase in job opportunities from information technology, aerospace, manufacturing, and other sectors. This has led to the migration of a large population from different parts of the country to Bengaluru. There has been a significant increase in the number of buildings, houses, roads, metros, and other infrastructures, thereby widening the urban area.

It was found that the examination of LST patterns at different time frames can be effectively performed using hot spot analysis by Getis–Ord G_i^* statistics. The identification of hot spot and cold spot by this method does not depend on a single high or low LST value and, hence,

provides a better picture of the hot and cold regions. On the whole, hot spot regions (approximately 24%) are more compared to cold spot regions (approximately 14%). During the time period, hot spots have a tendency to decrease (39.56% in 1989 to 35.04% in 2017), while the cold spots tend to increase (14.36% in 1989 to 22.89% in 2017). As the urban expansion occurs, the cold spots have increased, and it is mainly clustered in the urban area. It confirms the presence of an urban cool island in Bengaluru urban district, where the surrounding rural area is warmer than the urban center.

The scope of the study is to characterize and establish a relationship between various land uses using multiregression analysis. The use of higher resolution satellite images can improve the result of LULC classification and thereby improve the analysis of LULC change.

In future land use planning, a sufficient proportion of public space, green area, and water should be provided in metropolitan cities to cater to the effect of climate change due to urbanization. This study provides a scientific basis for the land use planners and policy makers for the management of cities confronting rapid urban growth.

References

- Aldwaik, S. Z., & Pontius, R. G. (2012). Intensity analysis to unify measurements of size and stationarity of land changes by interval, category, and transition. *Landscape and Urban Planning*, 106(1), 103–114. <https://doi.org/10.1016/j.landurbplan.2012.02.010>.
- Arnfield, A. J. (2003). Two decades of urban climate research: a review of turbulence, exchanges of energy and water, and the urban heat island. *International Journal of Climatology*, 23(1), 1–26. <https://doi.org/10.1002/joc.859>.
- Asuero, A. G., Sayago, A., & González, A. G. (2006). The correlation coefficient: an overview. *Critical Reviews in Analytical Chemistry*, 36(1), 41–59. <https://doi.org/10.1080/10408340500526766>.
- Babazadeh, M., & Kumar, P. (2015). Estimation of the urban Heat Island in local climate change and vulnerability assessment for air quality in Delhi. *European Scientific Journal*, 7881(June), 55–65.
- Balzter, H., Weng, Q., Sobrino, J., Smith, C., Rasul, A., Adamu, B., et al. (2017). A review on remote sensing of urban heat and cool islands. *Land*, 6(2), 38. <https://doi.org/10.3390/land6020038>.
- Bendib, A., Dridi, H., & Kalla, M. I. (2017). Contribution of Landsat 8 data for the estimation of land surface temperature in Batna city, eastern Algeria. *Geocarto International*, 32(5), 503–513. <https://doi.org/10.1080/10106049.2016.1156167>.
- Bhat, P. A., Shafiq, M. u., Mir, A. A., & Ahmed, P. (2017). Urban sprawl and its impact on landuse/land cover dynamics of Dehradun City, India. *International Journal of Sustainable*

- Built Environment*, 6(2), 513–521. <https://doi.org/10.1016/j.ijsbe.2017.10.003>.
- Chakraborty, S. D., Kant, Y., & Mitra, D. (2015). Assessment of land surface temperature and heat fluxes over Delhi using remote sensing data. *Journal of Environmental Management*, 148, 143–152. <https://doi.org/10.1016/j.jenvman.2013.11.034>.
- Chaudhuri, G., & Mishra, N. B. (2016). Spatio-temporal dynamics of land cover and land surface temperature in Ganges-Brahmaputra delta: a comparative analysis between India and Bangladesh. *Applied Geography*, 68, 68–83. <https://doi.org/10.1016/j.apgeog.2016.01.002>.
- Cohen, J. (1960). A coefficient of agreement for nominal scales. *Educational Psychology Measurement*, 20, 37–46.
- Congalton, R. G. (1991). A review of assessing the accuracy of classifications of remotely sensed data. *Remote Sensing of Environment*, 37, 35–46. [https://doi.org/10.1016/0034-4257\(91\)90048-B](https://doi.org/10.1016/0034-4257(91)90048-B).
- Craglia, M., Haining, R., & Wiles, P. (2000). A comparative evaluation of approaches to urban crime pattern analysis. *Urban Studies*, 37(4), 711–729.
- Devadas, M. D., & Rose, L. A. (2009). Urban factors and the intensity of Heat Island in the city of Chennai. In: *Proc. of the seventh International Conf. on Urban Climate*, p. 3–6.
- ESRI, (2017). *How hot spot analysis (Getis-Ord Gi*) works?* <http://pro.arcgis.com/en/pro-app/tool-reference/spatial-statistics/h-how-hot-spot-analysis-getis-ord-gi-spatial-stati.htm>. Accessed on 8th February 2017.
- Fan, C., Myint, S. W., Kaplan, S., Middel, A., Zheng, B., Rahman, A., et al. (2017). Understanding the impact of urbanization on surface urban heat islands—a longitudinal analysis of the oasis effect in subtropical desert cities. *Remote Sensing*, 9(7). <https://doi.org/10.3390/rs9070672>.
- Faris, A. A., & Reddy, Y. S. (2010). Estimation of urban heat island using Landsat-7 ETM+ 259 imagery at Chennai city—a case study. *International Journal of Earth Sciences and Engineering*, 3(3), 332–340.
- Foody, G. M. (2002). Status of land cover classification accuracy assessment. *Remote Sensing of Environment*, 80(1), 185–201. [https://doi.org/10.1016/S0034-4257\(01\)00295-4](https://doi.org/10.1016/S0034-4257(01)00295-4).
- Franco, S., Mandla, V. R., Rao, K. R. M., Kumar, M. P., & Anand, P. C. (2015). Study of temperature profile on various land use and land cover for emerging heat island. *Journal of Urban and Environmental Engineering*, 9(1), 32–37. <https://doi.org/10.4090/juee.2015.v9n1.032037>.
- Frey, C. M., Rigo, G., & Parlow, E. (2009). Investigation of the daily urban cooling island (UCI) in two coastal cities in an arid environment: Dubai and Abu Dhabi (UAE). *City*, 81, 2.06.
- Ghosh, S., Shastri, H., Sadavarte, P., Barik, B., & Venkataraman, C. (2017). Flip flop of day-night and summer-winter surface urban heat island intensity in India. *Scientific Reports*, 7(1). <https://doi.org/10.1038/srep40178>.
- Grover, A., & Singh, R. (2015). Analysis of urban heat island (UHI) in relation to normalized difference vegetation index (NDVI): a comparative study of Delhi and Mumbai. *Environments*, 2(4), 125–138. <https://doi.org/10.3390/environments2020125>.
- Harris, N. L., Goldman, E., Gabris, C., Nordling, J., Minnemeyer, S., Ansari, S., Lippmann, M., Bennett, L., Raad, M., Hansen, M., & Potapov, P. (2017). Using spatial statistics to identify emerging hot spots of forest loss using spatial statistics to identify emerging hot spots of forest loss. *Environmental Research Letters*, 12.
- Huang, J., Pontius, R. G., Li, Q., & Zhang, Y. (2012). Use of intensity analysis to link patterns with processes of land change from 1986 to 2007 in a coastal watershed of southeast China. *Applied Geography*, 34, 371–384. <https://doi.org/10.1016/j.apgeog.2012.01.001>.
- Jalan, S., & Sharma, K. (2014). Spatio-temporal assessment of land use/land cover dynamics and urban heat island of Jaipur city using satellite data. *International Archives of the Photogrammetry, Remote Sensing and Spatial Information Sciences - ISPRS Archives*, XL-8(1), 767–772. <https://doi.org/10.5194/isprsarchives-XL-8-767-2014>.
- Jiménez-Muñoz, J. C., & Sobrino, J. A. (2003). A generalized single-channel method for retrieving land surface temperature from remote sensing data. *Journal of Geophysical Research*, 108, 4688–4695.
- Kotharkar, R., & Surawar, M. (2015). Land use, land cover, and population density impact on the formation of canopy urban heat islands through traverse survey in the Nagpur urban area, India. *Journal of Urban Planning and Development*, 142(1), 04015003. [https://doi.org/10.1061/\(asce\)up.1943-5444.0000277](https://doi.org/10.1061/(asce)up.1943-5444.0000277).
- Landsat, N.A.S.A. (7) (2011). *Science data users handbook*. 2011-03-11. http://landsathandbook.gsfc.nasa.gov/inst_cal/prog_sect8_2.html. Accessed on 12th December 2017.
- Landsat, N.A.S.A. (8) (2015). *Science data users handbook*. 2015-June. <http://landsat.usgs.gov/l8handbook.php>. Accessed on 12th December 2017.
- Li, S., Mo, H., & Dai, Y. (2011). Spatio-temporal pattern of urban cool island intensity and its eco-environmental response in Chang-Zhu-Tan urban agglomeration. *Communications in Information Science Management and Engineering*, 1(9), 1–6.
- Li, Z. L., Tang, B. H., Wu, H., Ren, H., Yan, G., Wan, Z., Trigo, I. F., & Sobrino, J. A. (2013). Satellite-derived land surface temperature: current status and perspectives. *Remote Sensing of Environment*, 131, 14–37. <https://doi.org/10.1016/j.rse.2012.12.008>.
- Li, B., Wang, W., Bai, L., Wang, W., & Chen, N. (2018). Effects of spatio-temporal landscape patterns on land surface temperature: a case study of Xi'an city, China. *Environmental Monitoring and Assessment*, 190(7), 419. <https://doi.org/10.1007/s10661-018-6787-z>.
- Liu, G., Zhang, Q., Li, G., & Doronzo, D. M. (2016). Response of land cover types to land surface temperature derived from Landsat-5 TM in Nanjing metropolitan region, China. *Environmental Earth Sciences*, 75(20), 1–12. <https://doi.org/10.1007/s12665-016-6202-4>.
- Manandhar, R., Odeh, I., & Pontius, R. G. (2010). Analysis of twenty years of categorical land transitions in the lower hunter of New South Wales, Australia. *Agriculture, Ecosystems and Environment*, 135, 336–346.
- Mathew, A., Khandelwal, S., & Kaul, N. (2016). Spatial and temporal variations of urban heat island effect and the effect of percentage impervious surface area and elevation on land surface temperature: study of Chandigarh city, India. *Sustainable Cities and Society*, 26, 264–277. <https://doi.org/10.1016/j.scs.2016.06.018>.

- McCarville, D., Buenemann, M., Bleiweiss, M., & Barsi, J. (2011). *Atmospheric correction of Landsat thermal infrared data: a calculator based on North American Regional Reanalysis (NARR) data* (p. 12). In: Proc. of the American Society for Photogrammetry and Remote Sensing Conf.
- Nelson, T. A., & Boots, B. (2008). Detecting spatial hot spots in landscape ecology. *Ecography*, *31*(5), 556–566. <https://doi.org/10.1111/j.0906-7590.2008.05548.x>.
- Ogawa, K., Gurjar, B. R., Kikegawa, Y., Mohan, M., Kandya, A., & Bhati, S. (2012). Urban heat island assessment for a tropical urban airshed in India. *Atmospheric and Climate Sciences*, *02*(02), 127–138. <https://doi.org/10.4236/acs.2012.22014>.
- Ord, J. K., & Getis, A. (1995). Local spatial autocorrelation statistics: distributional issues and an application. *Geographical Analysis*, *27*(4), 286–306.
- Pal, S., & Ziaul, S. (2017). Detection of land use and land cover change and land surface temperature in English Bazar urban centre. *Egyptian Journal of Remote Sensing and Space Science*, *20*(1), 125–145. <https://doi.org/10.1016/j.ejrs.2016.11.003>.
- Prasannakumar, V., Vijith, H., Charutha, R., & Geetha, N. (2011). Spatio-temporal clustering of road accidents: GIS based analysis and assessment. *Procedia - Social and Behavioral Sciences*, *21*, 317–325. <https://doi.org/10.1016/j.sbspro.2011.07.020>.
- Qin, Z., Karnieli, A., & Berliner, P. (2001). A mono-window algorithm for retrieving land surface temperature from Landsat TM data and its application to the Israel-Egypt border region. *International Journal of Remote Sensing*, *22*(18), 3719–3746. <https://doi.org/10.1080/01431160010006971>.
- Ramachandra, T. V., & Kumar, U. (2009). Land surface temperature with land cover dynamics: multi-resolution, spatio-temporal data analysis of Greater Bangalore, India. *International Journal of Geoinformatics*, *5*(3), 43–53.
- Ramachandra, T. V., Aithal, B. H., Vinay, S., Joshi, N. V., Kumar, U., & Rao, V. K. (2013). *Modelling urban revolution in Greater Bangalore, India. 30th Annual In-House Symposium on Space Science and Technology, ISRO-IISc Space Technology Cell* (pp. 1–5). Bangalore: Indian Institute of Science.
- Rasul, A., Balzter, H., & Smith, C. (2015). Urban climate spatial variation of the daytime surface urban cool island during the dry season in Erbil, Iraqi Kurdistan, from Landsat 8. *Urban Climate*, *14*, 176–186. <https://doi.org/10.1016/j.uclim.2015.09.001>.
- Rasul, A., Balzter, H., & Smith, C. (2017). Applying a normalized ratio scale technique to assess influences of urban expansion on land surface temperature of the semi-arid city of Erbil. *International Journal of Remote Sensing*, *38*(13), 3960–3980. <https://doi.org/10.1080/01431161.2017.1312030>.
- Shi, Y., & Zhang, Y. (2018). Remote sensing retrieval of urban land surface temperature in hot-humid region. *Urban Climate*, *24*, 299–310. <https://doi.org/10.1016/j.uclim.2017.01.001>.
- Smits, P. C., Dellepiane, S. G., & Schowengerdt, R. A. (1999). Quality assessment of image classification algorithms for land-cover mapping: a review and a proposal for a cost-based approach. *International Journal of Remote Sensing*, *20*(8), 1461–1486. <https://doi.org/10.1080/014311699212560>.
- Sudhira, H. S., Ramachandra, T. V., & Subrahmanya, M. H. B. (2007). Bangalore. *Cities*, *24*(5), 379–390. <https://doi.org/10.1016/j.cities.2007.04.003>.
- Tan, K. C., Lim, H. S., MatJafri, M. Z., & Abdullah, K. (2010). Landsat data to evaluate urban expansion and determine land use/land cover changes in Penang Island, Malaysia. *Environmental Earth Sciences*, *60*(7), 1509–1521. <https://doi.org/10.1007/s12665-009-0286-z>.
- Tran, D. X., Pla, F., Latorre-Carmona, P., Myint, S. W., Caetano, M., & Kieu, H. V. (2017). Characterizing the relationship between land use land cover change and land surface temperature. *ISPRS Journal of Photogrammetry and Remote Sensing*, *124*, 119–132. <https://doi.org/10.1016/j.isprsjprs.2017.01.001>.
- Valor, E., & Caselles, V. (1996). Mapping land surface emissivity from NDVI: application to European, African, and South American areas. *Remote Sensing of Environment*, *57*(3), 167–184. [https://doi.org/10.1016/0034-4257\(96\)00039-9](https://doi.org/10.1016/0034-4257(96)00039-9).
- Wolf, T., & McGregor, G. (2013). The development of a heat wave vulnerability index for London, United Kingdom. *Weather and Climate Extremes*, *1*, 59–68. <https://doi.org/10.1016/j.wace.2013.07.004>.
- Zhang, Y., Fu, Y., Kong, X., & Zhang, F. (2019). Prefecture-level city shrinkage on the regional dimension in China: spatio-temporal change and internal relations. *Sustainable Cities and Society*, *47*(February), 101490. <https://doi.org/10.1016/j.scs.2019.101490>.
- Zhao, R., Chen, Y., Shi, P., Zhang, L., Pan, J., & Zhao, H. (2013). Land use and land cover change and driving mechanism in the arid inland river basin: a case study of Tarim River, Xinjiang, China. *Environmental Earth Sciences*, *68*(2), 591–604. <https://doi.org/10.1007/s12665-012-1763-3>.
- Zhou, D. C., Zhao, S. Q., Liu, S. G., Zhang, L. X., & Zhu, C. (2014). Surface urban heat island in China's 32 major cities: spatial pattern and drivers. *Remote Sensing of Environment*, *152*, 51–61.
- Ziaul, S., & Pal, S. (2018). Anthropogenic heat flux in English Bazar town and its surroundings in West Bengal, India. *Remote Sensing Applications: Society and Environment*, *11*, 151–160. <https://doi.org/10.1016/j.rsase.2018.06.003>.

Publisher's note Springer Nature remains neutral with regard to jurisdictional claims in published maps and institutional affiliations.